Oncogene (2007) 26, 6010–6020

www.nature.com/onc

ORIGINAL ARTICLE

The nonhomologous end joining factor Artemis suppresses multi-tissue tumor formation and prevents loss of heterozygosity

Y Woo[1,2,7], SM Wright[1,7], SA Maas[1,7], TL Alley[1], LB Caddle[1], S Kamdar[1], J Affourtit[1], O Foreman[1], EC Akeson[1], D Shaffer[1,3], RT Bronson[1,4,5], HC Morse III[6], D Roopenian[1,3] and KD Mills[1]

[1]*The Jackson Laboratory, Bar Harbor, ME, USA;* [2]*Functional Genomics PhD Program, University of Maine, Orono, ME, USA;* [3]*Bar Harbor Biotechnology, Trenton, ME, USA;* [4]*Department of Biomedical Sciences, Cummings School of Veterinary Medicine, Tufts University, North Grafton, MA, USA;* [5]*Department of Pathology, Harvard University Medical School, Boston, MA, USA and* [6]*Laboratory of Immunopathology, National Institute of Allergy and Infectious Diseases, Rockville, MD, USA*

Nonhomologous end joining (NHEJ) is a critical DNA repair pathway, with proposed tumor suppression functions in many tissues. Mutations in the NHEJ factor ARTEMIS cause radiation-sensitive severe combined immunodeficiency in humans and may increase susceptibility to lymphoma in some settings. We now report that deficiency for Artemis (encoded by *Dclre1c/Art* in mouse) accelerates tumorigenesis in several tissues in a *Trp53* heterozygous setting, revealing tumor suppression roles for NHEJ in lymphoid and non-lymphoid cells. We also show that B-lineage lymphomas in these mice undergo loss of *Trp53* heterozygosity by allele replacement, but arise by mechanisms distinct from those in *Art Trp53* double null mice. These findings demonstrate a general tumor suppression function for NHEJ, and reveal that interplay between NHEJ and *Trp53* loss of heterozygosity influences the sequence of multi-hit oncogenesis. We present a model where p53 status at the time of tumor initiation is a key determinant of subsequent oncogenic mechanisms. Because *Art* deficient mice represent a model for radiation-sensitive severe combined immunodeficiency, our findings suggest that these patients may be at risk for both lymphoid and non-lymphoid cancers.
Oncogene (2007) **26,** 6010–6020; doi:10.1038/sj.onc.1210430; published online 26 March 2007

Keywords: nonhomologous end joining; RS-SCID; Artemis; loss of heterozygosity; p53

Introduction

Nonhomologous end joining (NHEJ) is a critical pathway for DNA double strand break (DSB) repair in eukaryotic cells. Cells with mutations in NHEJ genes exhibit chromosomal instability, hypersensitivity to ionizing radiation (IR), increased cellular senescence and proliferation defects, indicative of defects in the repair of spontaneous and induced DSBs (Ferguson and Alt, 2001; Jackson, 2002; Jeggo and Lobrich, 2006). Mice with deficiencies in six of the seven known NHEJ factors have been isolated or engineered and show phenotypes ranging from variable B-, T-severe combined immunodeficiency (SCID), to IR sensitivity, to late embryonic lethality associated with extensive neuronal apoptosis (reviewed in Mills *et al*., 2003; Rooney *et al*., 2004a). In humans, mutant alleles in the gene encoding the NHEJ factor ARTEMIS are the molecular basis for radiation-sensitive SCID (RS-SCID), and hypomorphic *ARTEMIS* alleles may be associated with increased lymphoma predisposition (Nicolas *et al*., 1998; Moshous *et al*., 2001, 2003; Ege *et al*., 2005). The importance of NHEJ in genomic stability suggests that this pathway should suppress tumors in many somatic tissues, but roles for NHEJ in tumor suppression have primarily been characterized in B-lymphocytes.

Loss of heterozygosity (LOH) is a common genetic aberration in both sporadic and familial cancers (reviewed in Tischfield and Shao, 2003). The critical tumor suppressor p53 (encoded by *TP53* in humans and *Trp53* in mice) is mutated in greater than half of all inherited and spontaneously arising human cancers, often through LOH. The importance of p53 is underscored by mouse studies showing that homozygous inactivation of the *Trp53* gene results in the dramatic increase in broad-spectrum tumor incidence (Donehower *et al*., 1992; Jacks *et al*., 1994; Harvey *et al*., 1993). Although the molecular mechanisms for LOH are poorly defined, DSBs have been suggested as initiating lesions, especially for deletional or recombinational mechanisms (Jasin, 2000; Lasko *et al*., 1991; Stark and Jasin, 2003). This is supported by the observation that IR is associated with *Trp53* LOH, leading to accelerated tumorigenesis in $Trp53^{N/+}$ mice (Jiang *et al*., 2001; Liang *et al*., 2002). In this context, specific functions of DSB repair pathways to prevent LOH are unknown.

Correspondence: Dr KD Mills, The Jackson Laboratory, 600 Main Street, Bar Harbor, ME 04609, USA.
E-mail: kevin.mills@jax.org
[7]These authors contributed equally to this work.
Received 13 December 2006; revised 8 February 2007; accepted 9 February 2007; published online 26 March 2007

We now report that Artemis deficiency accelerates tumorigenesis in several tissues and shifts the tumor spectrum in $Trp53^{N/+}$ mice, demonstrating a multi-tissue tumor suppression function for NHEJ. In addition to non-lymphoid tumors, *Art* null *Trp53* heterozygous mice (hereafter denoted $Art^{N/N}Trp53^{N/+}$) developed B lineage lymphomas reminiscent of those arising in NHEJ/*Trp53* double null mice. These lymphomas showed LOH at *Trp53*, but, surprisingly, exhibited cytogenetic and molecular abnormalities distinct from those in NHEJ/*Trp53* double null mice. We present a model for the interplay of NHEJ and *Trp53* LOH, wherein p53 status at the time of initiation is a key determinant in the timing and order of multi-hit oncogenesis.

Results

NHEJ suppresses tumor formation in multiple tissues

While generating lymphoma-prone *Art Trp53* double null mice ($Art^{N/N}Trp53^{N/N}$), we unexpectedly observed that a subset of the breeder $Art^{N/N}Trp53^{N/+}$ mice developed tumors with latency similar to those in double null mice. To characterize subsequently the transformation mechanisms, a total of 71 $Art^{N/N}Trp53^{N/+}$ mice were generated, together with 33 $Art^{N/N}Trp53^{N/N}$ and 39 $Trp53^{N/+}$ controls.

All mice were monitored for a minimum of 45 weeks, with some $Art^{N/N}Trp53^{N/+}$ mice followed for up to 66 weeks. During the main 45-week observation window 13 of the $Art^{N/N}Trp53^{N/+}$ mice (20%) succumbed, and in total, 24 $Art^{N/N}Trp53^{N/+}$ mice (34%) developed illness and were euthanized for analysis. Nine (9) lymphomas, two (2) anaplastic sarcomas, five (5) differentiated sarcomas and two (2) malignant gliomas were observed as well as several non-malignant pathologies. By contrast, none of the 39 control $Trp53^{N/+}$ mice developed illness during the observation period, and statistical comparisons revealed the $Art^{N/N}Trp53^{N/+}$ and $Trp53^{N/+}$ survival data sets to be highly significantly different ($P = 0.005$). Finally, the $Art^{N/N}Trp53^{N/+}$ mice succumbed at a median age of 48 weeks, as compared with 62–64 weeks for $Trp53^{N/+}$ mice (Figure 1a; Table 1). Consistent with previously published data, all (33/33) $Art^{N/N}Trp53^{N/N}$ mice rapidly developed fulminant lymphoma and succumbed by 16 weeks (Rooney *et al*., 2004b). No $Art^{N/N}Trp53^{+/+}$ mice developed tumors during this study, consistent with previous reports (Rooney *et al*., 2002).

To investigate the mechanistic basis for tumor development in $Art^{N/N}Trp53^{N/+}$ mice, detailed molecular and cytogenetic analyses were performed for three lymphomas and two sarcomas that were separable from surrounding normal tissue. Two of the lymphomas (AP546 and AP1605) presented as large focal lesions affecting multiple lymph nodes, whereas the third lymphoma (AP1043) presented as numerous discrete lesions primarily in the spleen and some lymph nodes. Flow cytometry (Figure 1c; Supplementary Figure 1) and Southern blot analyses (Supplementary Figure 2) demonstrated that the lymphomas in $Art^{N/N}Trp53^{N/+}$ mice, like those in $Art^{N/N}Trp53^{N/N}$ mice, arose in the B-lineage, likely at the progenitor stage of development.

Overt Trp53 *LOH occurs in lymphomas, but not sarcomas, in* $Art^{N/N}Trp53^{N/+}$ *mice*

Because *Trp53* LOH is commonly observed in a variety of spontaneous and induced mouse tumors, we tested whether the wild type *Trp53* allele was lost in the three $Art^{N/N}Trp53^{N/+}$ lymphomas (AP546, AP1043 and AP1605) and two $Art^{N/N}Trp53^{N/+}$ sarcomas (AP1134 and AP1454) (Figure 2a). PCR genotype analysis revealed loss of the wild type *Trp53* allele in all three lymphomas but not the sarcomas. One lymphoma (AP1043) contained an additional lymph node tumor focus, which showed both wild type and null *Trp53* alleles, suggesting an independently arising lymphoma with different p53 status in this mouse (Figure 2a). However, array comparative genomic hybridization (CGH) revealed that all tumor foci from this mouse contained similar copy number abnormalities (CNAs) (data not shown), indicating that contaminating non-tumor tissue likely contributed the wild-type *Trp53* allele in this case. By contrast to the lymphomas, both sarcoma samples retained an intact wild-type *Trp53* allele (Figure 2a). These results indicate that, unlike the lymphomas, the formation of sarcomas in the absence of *Art* was not accompanied by overt loss of the wild-type *Trp53* allele. Although it is possible that the wild-type band in the sarcomas was owing to contaminating normal tissue, this is not likely because, in both instances, DNA was isolated from tumor masses distinct and separate from adjacent normal tissue. However, we cannot rule out functional inactivation of p53 by other mechanisms not detected by this PCR strategy. Together, these data demonstrate that B lineage lymphomagenesis in $Art^{N/N}Trp53^{N/+}$ mice was accompanied by LOH for *Trp53* in most, if not all, cases (hereafter denoted $Art^{N/N}Trp53^{LOH}$).

Loss of Trp53 *heterozygosity in lymphomas occurs by an allele replacement mechanism*

To determine whether *Trp53* LOH resulted from a large interstitial deletion or other cytogenetic abnormality, fluorescence *in situ* hybridization (FISH) analysis was performed (Figure 2b and c). Metaphase chromosome spreads were prepared for the AP546 and AP1605 lymphomas, co-stained with a chromosome (Chr) 11-specific paint and a fluorescently labeled BAC probe containing the *Trp53* locus and counterstained with DAPI (Figure 2b and c). Neither AP1605 nor AP546 showed evidence of a deletion affecting *Trp53* on either allele, but in AP546 one *Trp53* allele appeared near the junction of a translocation, shown by spectral karyotype (SKY) analysis to be a nonreciprocal der(11)t(1;11) (Figures 2b, c and 4g). Additional FISH mapping suggested that the translocation junction in this tumor was located within a BAC length (~200 kilobase pairs) proximal to *Trp53* and that Chr 11 sequences proximal

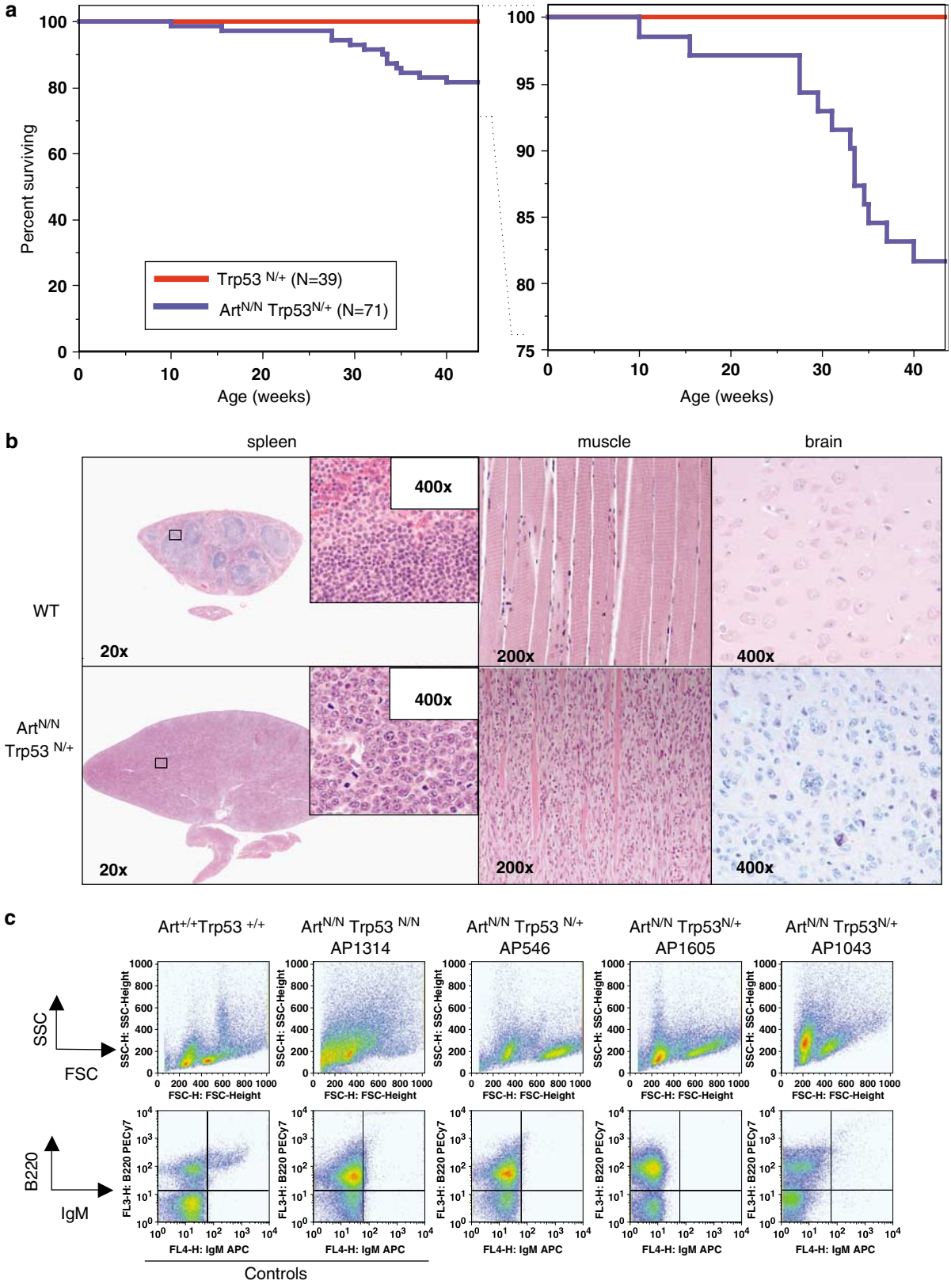

Figure 1 Artemis deficiency leads to accelerated tumorigenesis in a *Trp53* heterozygous context. (**a**) Kaplan–Meier plot showing percent survival for $Art^{N/N}Trp53^{N/+}$ and $Trp53^{N/+}$ mice. Statistical testing was performed by log–rank test ($P=0.005$). (**b**) Representative histology of indicated H&E stained tissue sections from normal (top panels) or $Art^{N/N}Trp53^{N/+}$ mice (bottom panels). Shown are spleen ($\times 20$ and $\times 400$ from boxed area), muscle ($\times 200$) and brain ($\times 400$). (**c**) Flow cytometric analysis of lymphomas in $Art^{N/N}Trp53^{N/+}$ mice (AP546, AP1605 and AP1043), and controls. Shown are ungated side-scatter versus forward-scatter (top panels) and B220 versus IgM (bottom panels) plots.

Table 1 Tumor Histopathology in $Art^{N/N}/Trp53^{N/+}$, $Trp53^{N/+}$ and $Trp53^{N/N}$ mice. Histological findings and the percentage of total tumors as well as median age of death in weeks are listed

	Pathology	N	*% of total tumors*	*Median age at death (wks)*
$Art^{N/N}$ $Trp53^{N/+}$				
	Lymphoma	9	50	
	Malignant glioma	2	11	
	Differentiated sarcoma	5	28	
	Anaplastic sarcoma	2	11	**48**
	Non-malignant	6	NA	
	No abnormalities	1	NA	
$Trp53^{N/+}$				
Harvey *et al*. (1993)	Differentiated sarcoma	*See ref*.	41	
	Lymphoma	*See ref*.	32	~62
	Anaplastic sarcoma	*See ref*.	3	
	Carcinoma	*See ref*.	12	
	Other	*See ref*.	2	
Jacks *et al*. (1994)	Sarcoma	*See ref*.	57	
	Lymphoma	*See ref*.	25	~64
	Carcinoma	*See ref*.	11	
	Other	*See ref*.	5	
$Trp53^{N/N}$				
Harvey *et al*. (1993)	Differentiated sarcoma	*See ref*.	21	
	Lymphoma	*See ref*.	59	~20
	Anaplastic sarcoma	*See ref*.	5	
	Carcinoma	*See ref*.	2	
	Other	*See ref*.	13	

to this junction were amplified (Figure 2b; Supplementary Figure 3). Together, these data ruled out large scale deletion and suggested that *Trp53* LOH occurred either by small focal deletion or by allele replacement, rather than by large-scale deletion.

To distinguish between deletion and allele replacement LOH mechanisms, a quantitative PCR strategy (Q-PCR) was devised to measure the copy number of wild type versus knockout alleles (i.e. 0, 1, 2 or more copies per cell) (Figure 3a). Primers were designed to detect either a *Trp53* knockout allele specific sequence (NEO), or a *Trp53* locus sequence common to both the wild type and null alleles (COMMON). To calibrate this approach, $Trp53^{+/+}$ and $Trp53^{N/N}$ DNA samples were mixed at defined ratios, and either NEO or COMMON sequences were evaluated (Figure 3b; Supplementary methods). This demonstrated both linearity and sensitivity for the assay, showing that various ratios of NEO: COMMON sequences could be accurately quantified (Figure 3b). Analysis of the AP546 and AP1605 lymphomas by this method confirmed the presence of the null allele and absence of the normal *Trp53*. To discriminate between deletion and replacement of the normal *Trp53* allele, the assay was repeated, comparing ΔC_t values for NEO or COMMON sequences against a series of four unaffected 'normalizer' genes. Control samples showed NEO and COMMON sequences, both present in two copies (Figure 3c). Analysis of tail DNA from AP1605 produced $\Delta C_{tCOMMON}$ values near zero (0), and ΔC_{tNEO} values close to 1 as expected, (Figure 3c). By contrast, $Art^{N/N}Trp53^{LOH}$ lymphomas AP546 and AP1605 contained two copies of both NEO and COMMON sequences, indicating replacement of the wild type with the knockout allele (Figure 3b and c). Analysis of tumor and non-tumor DNA from AP1043 revealed Chr 11 instability even in non-lymphoid tissues, precluding an accurate assessment of *Trp53* copy number changes between germline and tumor.

Cytogenetic lesions differ in $Art^{N/N}Trp53^{LOH}$ *versus* $Art^{N/N}Trp53^{N/N}$ *lymphomas*

$Art^{N/N}Trp53^{N/N}$ tumors typically show one of two characteristic patterns of chromosomal abnormalities: (1) a der(12) t(12;15) translocation and a complex der(15) complicon, harboring co-amplified *c-myc* and *Igh* loci; or (2) a der(12) complicon harboring co-amplified *N-myc* and *Igh* loci (Zhu *et al*., 2002; Rooney *et al*., 2004b). $Art^{N/N}Trp53^{LOH}$ tumors were tested for similar cytogenetic lesions, employing SKY analysis to evaluate chromosomal translocations (Figure 4). $Art^{N/N}Trp53^{N/N}$ tumors showed expected translocation patterns typifying either *c-myc* or *N-myc* complicons (Figure 4a–d; Supplementary Figure 4). By contrast, $Art^{N/N}Trp53^{LOH}$ tumors AP546 and AP1605 lacked the der(15) translocation associated with complicons, and instead contained variant translocations. AP546 contained a nonreciprocal der(12)t(5;12) translocation, but lacked any Chr 15 translocations (Figure 4e–h). FISH analysis identified a translocation that juxtaposed the *Igh* and *c-myc* loci, revealing low level amplification of *c-myc* but not of *Igh*. SKY data indicate that the juxtaposed *Igh* and *c-myc* loci likely occur on the der(12)t(5;12) chromosome, a structure not observed in $Art^{N/N}Trp53^{N/N}$

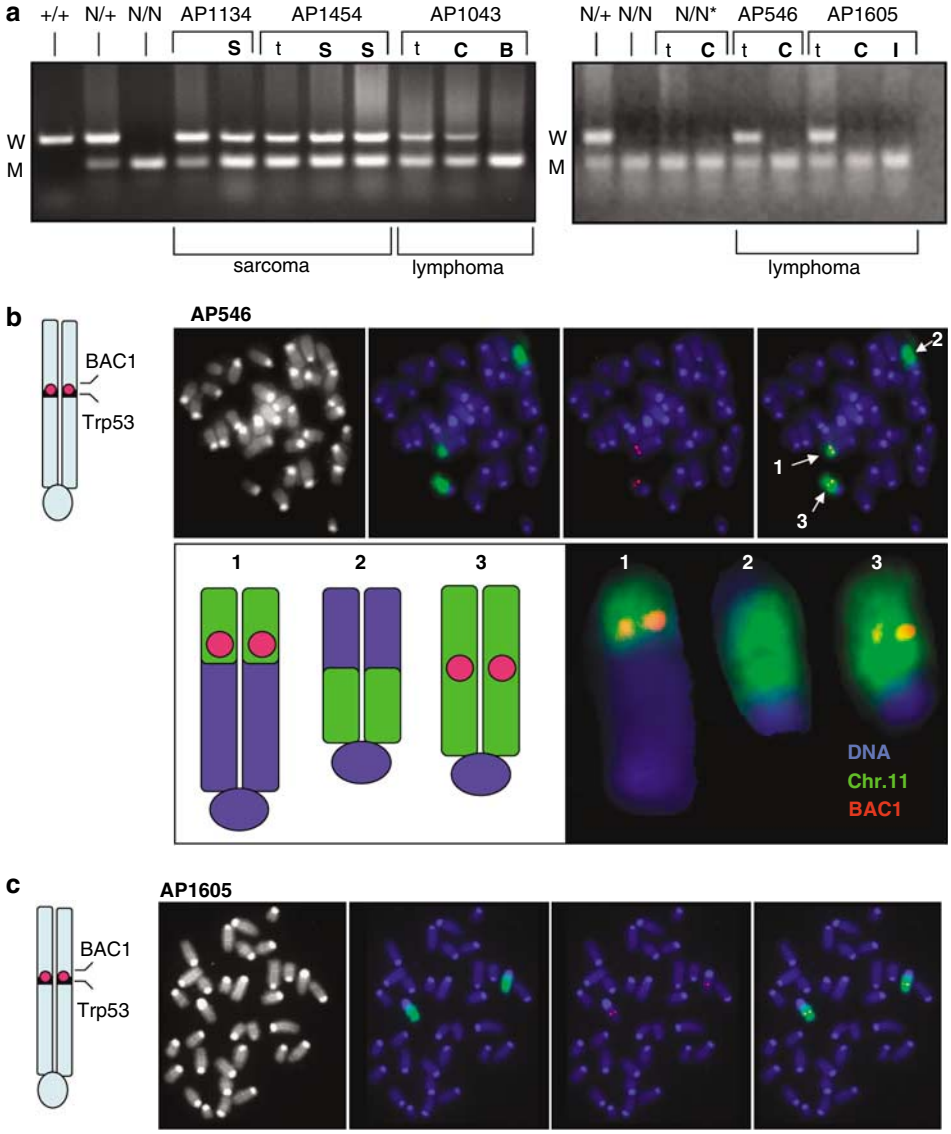

Figure 2 Lymphomas from $Art^{N/N}Trp53^{N/+}$ mice undergo loss of *Trp53* heterozygosity. (**a**) PCR genotype analysis of *Trp53* alleles in lymphomas (AP546, AP1605 and AP1043) and sarcomas (AP1454 and AP1134) from $Art^{N/N}Trp53^{N/+}$ mice. Tail DNA from unrelated $Trp53^{+/+}$, $Trp53^{N/+}$ or $Trp53^{N/N}$ mice and tail and tumor DNA from an $Art^{N/N}Trp53^{N/N}$ mouse (N/N*) were included as controls. Wild type (W) and mutant (M) alleles are indicated. t = tail; S = sarcoma; C = cervical lymph node; B = brachial lymph node; I = inguinal lymph node. (**b** and **c**) FISH analysis with Chr 11 paint (green) and the *Trp53* BAC1 probe (red) of lymphomas AP546 (**b**) and AP1605 (**c**). Chromosomes showing FISH signals are indicated with an arrow and shown diagrammatically on the left. DNA was counterstained with DAPI (blue), and color merged images are shown.

tumors. AP1605 contained a marker der(12) t(12;15) translocation, but likewise lacked a der(15) translocation or other apparent complicon-like structures (Figure 4i–l). Moreover, neither AP1605 nor AP546 showed a shortened or elongated Chr 12 typical of *N-myc* complicons in $Art^{N/N}Trp53^{N/N}$ mice (Supplementary Figure 4). Furthermore, *N-myc* amplification was not detected in these tumors by array CGH, Q-PCR, or Southern blot analysis (Figure 5c and d; Supplementary Figure 2) and overexpression of *N-myc* was not observed via Affymetrix GeneChip analysis (data not shown). Together, these data show that $Art^{N/N}Trp53^{LOH}$ lymphomas arise without either *c-myc* or *N-myc* complicons, mechanistically distinguishing them from $Art^{N/N}Trp53^{N/N}$ lymphomas.

Copy number aberrations differ in $Art^{N/N}Trp53^{LOH}$ *versus* $Art^{N/N}Trp53^{N/N}$ *lymphomas*

To test further whether the molecular etiology of $Art^{N/N}Trp53^{LOH}$ and $Art^{N/N}Trp53^{N/N}$ lymphomas differed, DNA copy number profiles were assayed by array CGH. By contrast with $Art^{N/N}Trp53^{N/N}$, no $Art^{N/N}Trp53^{LOH}$ tumor showed interstitial amplification at proximal Chr 12, and two of the three lymphomas (AP1043 and AP1605) lacked amplification on Chr 15, confirming the absence of *c-myc* complicons (Figure 5a–c). The third lymphoma (AP546) showed low-level (~4-fold) amplification on medial Chr 15 near *c-myc*, which was independently confirmed by Q-PCR using a high throughput 384-gene CancerQuantArray platform (D Roopenian and HC Morse, unpublished resources)

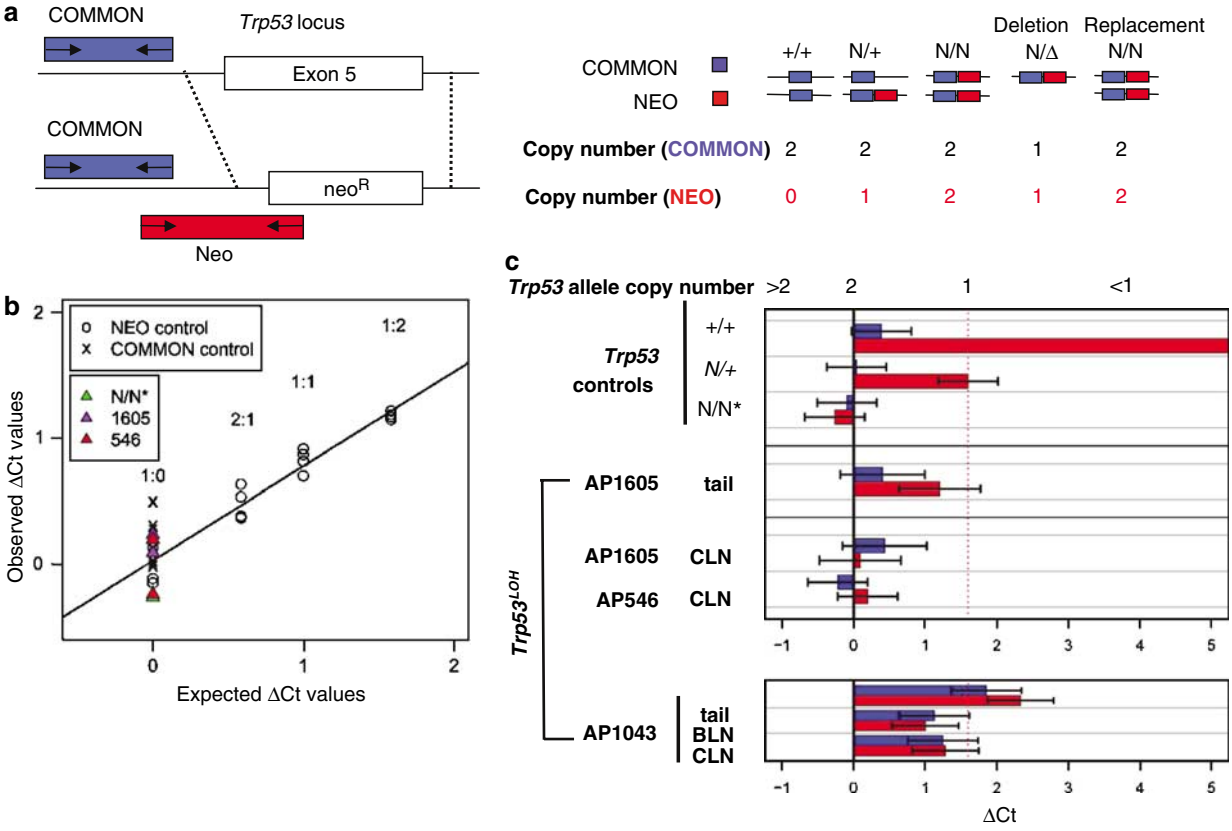

Figure 3 LOH occurs by allele replacement in $Art^{N/N}Trp53^{LOH}$ lymphomas. (**a**) Schematic showing quantitative PCR strategy to evaluate wild-type and knockout *Trp53* allele copy number. Possible copy number configurations to distinguish genotypes and different LOH mechanisms through common (blue) and neo (red) PCR product analysis are indicated (right). (**b**) Scatter plot showing expected and observed ΔC_t values for a range of mixed samples of $Trp53^{N/N}$ and $Trp53^{+/+}$ ($Trp53^{N/N}$: $Trp53^{+/+}$ = 1:0, 2:1, 1:1 and 1:2). $\Delta C_t = C_{tTEST} - C_{tN/N\ TAIL}$. Circles (O) and crosses (X) represent NEO and COMMON ΔCt values of mixture samples. Triangles (Δ) represent average NEO ΔC_t values for tumor samples. (**c**) Bar chart showing ΔC_t values in $Trp53^{+/+}$, $Trp53^{N/+}$ and $Trp53^{N/N}$ controls and in tail versus tumor tissue from AP1605, AP546 and AP1043 mice. Dashed red line indicates the baseline single copy difference. Error bars represent 95% confidence intervals.

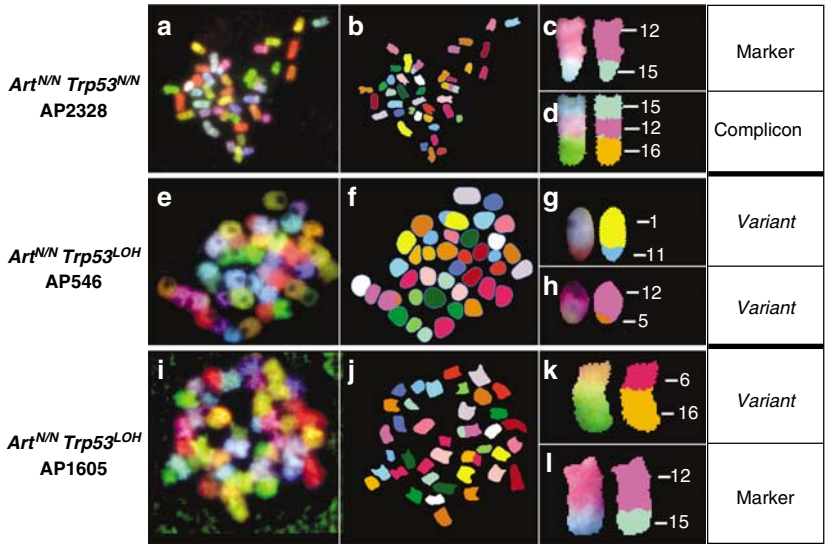

Figure 4 $Art^{N/N}Trp53^{LOH}$ lymphomas harbor variant cytogenetic lesions. SKY analysis of metaphase spreads from $Art^{N/N}Trp53^{N/N}$ lymphoma AP2328 (**a**–**d**) compared with $Art^{N/N}Trp53^{LOH}$ tumors AP546 (**e**–**h**), and AP1605 (**i**–**l**). Shown are spectral images of whole metaphase spreads (**a**, **e** and **i**), classified images of whole metaphase spreads (**b**, **f** and **j**) and expanded spectral plus classified views of clonal translocations observed in each tumor (**c**, **d**, **g**, **h**, **k** and **l**).

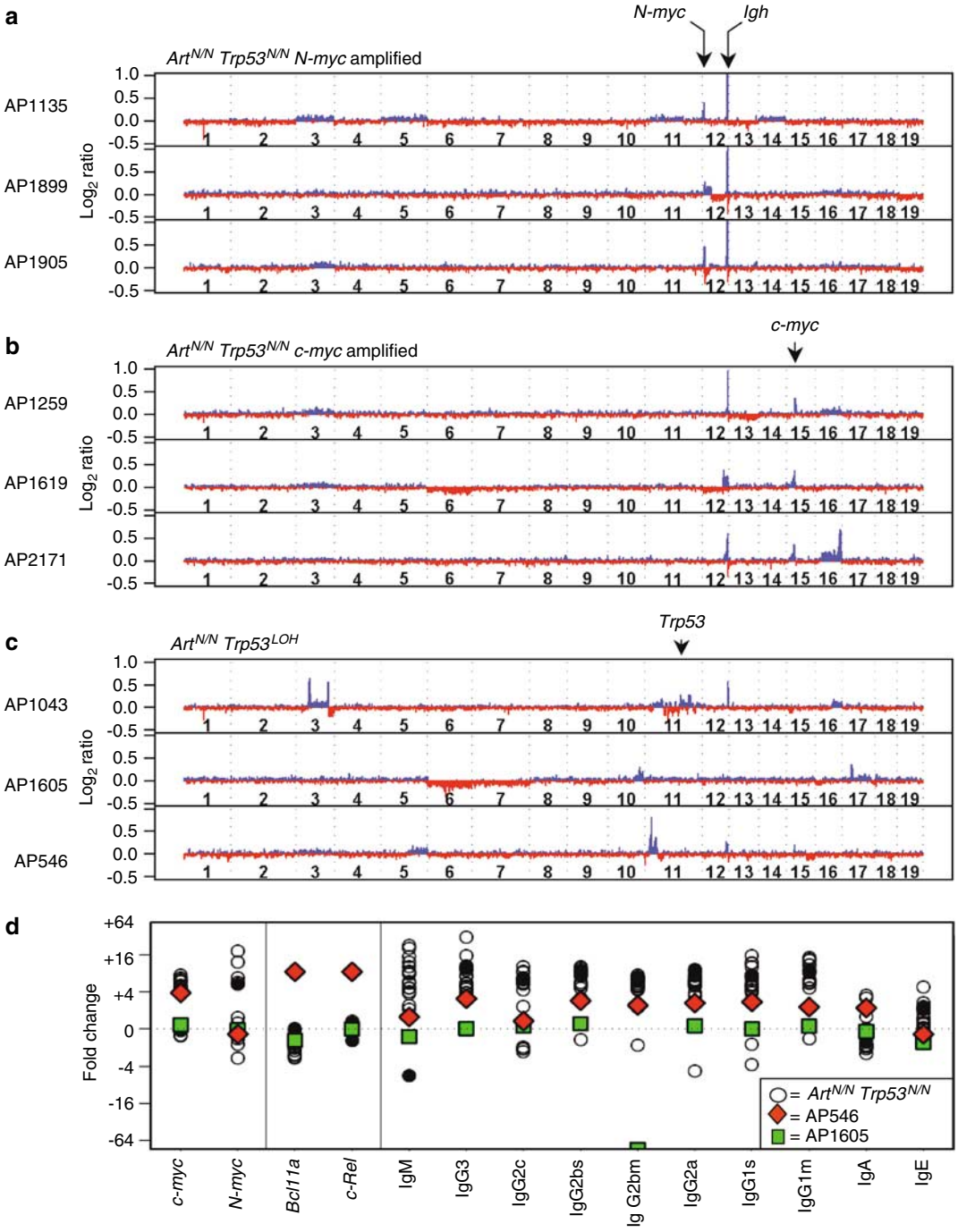

Figure 5 $Art^{N/N}Trp53^{LOH}$ lymphomas contain variant copy number abnormalities. Array CGH analysis showing quantile smoothed $\log_2$ (test/reference) data for three *N-myc* amplified $Art^{N/N}Trp53^{N/N}$ lymphomas (Eilers and de Menezes, 2005) (**a**), three *c-myc* amplified $Art^{N/N}Trp53^{N/N}$ lymphomas (**b**) and $Art^{N/N}Trp53^{LOH}$ tumors AP1043, AP1605 and AP546 tumors (**c**). Individual chromosomes are demarcated, and the $\log_2$ (test/reference) data were truncated at 1. The genomic locations of N-*myc*, *Igh*, *c-myc* and *Trp53* are marked. (**d**) Q-PCR analysis of CNAs at *c-myc*, *N-myc*, *Bcl11a*, *c-Rel* and *Igh* loci. The fold copy number change in tumors relative to normal C57BL/6J DNA is indicated.

(Figure 5d) (Akilesh *et al*., 2003). However, cytogenetic data demonstrated that this amplification was not associated either with a complicon or a simple translocation. Q-PCR also confirmed negligible amplification of *c-myc* and *Igh* in AP1605, supporting findings from CGH analysis (Figure 5d). Interestingly, the AP546 lymphoma showed substantial amplification of *Bcl11a* and *c-Rel*, both of which map within the Chr 11 amplicon detected by array CGH. Together with SKY and FISH data showing an associated translocation, these findings indicate that *Bcl11a* and *c-Rel*, but not *c-* or *N-myc*, were involved in a complicon in this tumor,

demonstrating that complicon formation is a general mechanism of gene amplification not restricted to *Igh* and *Myc*-family genes. Taken together, the cytogenetic and copy number analyses demonstrate that $Art^{N/N}Trp53^{LOH}$ lymphomas undergo tumor initiation or progression by molecular mechanisms that are distinct from those in $Art^{N/N}Trp53^{N/N}$ lymphomas.

Discussion

We have shown that the NHEJ factor Artemis (encoded by *Dclre1c*/*Art*) acts in concert with p53 to suppress tumor formation in multiple tissues, demonstrating the general importance of NHEJ in tumor suppression beyond the lymphoid system. Deficiency for *Artemis* in $Trp53^{N/+}$ mice both accelerated tumorigenesis and shifted the tumor spectrum associated with *Trp53* heterozygosity. In addition to lymphomas, $Art^{N/N}Trp53^{N/+}$ mice developed osteosarcomas, anaplastic sarcomas and a range of non-malignant pathologies. Importantly, two brain tumors, which have been very rarely linked with mouse *Trp53* deficiency but may be associated with human *TP53*-deficient syndromes, were observed in this study. Furthermore, lack of *Art* accelerated *Trp53* LOH, often by an allele replacement mechanism, in progenitor B-lymphocytes. Significantly, we demonstrate that lymphomas arising subsequent to *Trp53* LOH are not equivalent to those arising in mice that are fully null for *Trp53* in the germline. This surprising finding indicates that p53 status at the time of tumor initiation influences the sequence and the timing of subsequent oncogenic events.

NHEJ is a multi-tissue tumor suppression pathway

To date, most studies implicating NHEJ in tumor suppression have focused on lymphoid cells, but an important role for NHEJ has also been postulated in non-lymphoid tumor suppression. NHEJ has recently been associated, in certain tissue-specific cases, with non-lymphoid tumor suppression. Tissue-specific inactivation of *XRCC4* in *Trp53* deficient neuronal progenitor cells, or *Ku80*/*Trp53*/*Rag1* triple deficiency, both led to early onset medulloblastoma (Holcomb *et al*., 2006; Yan *et al*., 2006). Similarly, heterozygosity for *Lig4* in an *Ink4*/*Arf* null context led to accelerated formation of soft tissue sarcomas (Sharpless *et al*., 2001). However, these studies all required compound engineered mutations with concomitant germline inactivation of a tumor suppressor to create a highly sensitized system. Moreover, it is unclear whether *XRCC4* or *Lig4* nullizygosity in mouse relates to true clinical oncogenesis in humans, where such alleles have not been identified.

In this context, $Art^{N/N}Trp53^{N/+}$ mice represent a more clinically relevant disease model with implications for understanding human cancer-prone and immunodeficient syndromes, such as Li-Fraumeni and Li-Fraumeni-like syndromes (LFS and LFL, respectively) and radiation-sensitive (RS)-SCID. LFS and LFL are rare familial cancer syndromes characterized by predisposition to a wide spectrum of early onset tumors, including soft tissue sarcomas, breast cancer, adrenocortical carcinomas and brain tumors. Germline *TP53* mutations account for approximately 70% of LFS cancer diagnoses and have been implicated in some, but not all, LFL cases (reviewed in Olivier *et al*., 2003). Broad clinical heterogeneity, even within the same affected families, is often observed in both LFS and LFL, but the underlying reasons remain poorly understood. In this context, the latency and tumor spectrum in $Art^{N/N}Trp53^{N/+}$ mice, especially with respect to brain tumors, is reminiscent of some clinical features of LFS and LFL. Thus our data suggest that somatic DSB repair defects could influence the clinical heterogeneity and specific tumor development in some LFS or LFL patients and, in this regard, $Art^{N/N}Trp53^{N/+}$ mice may represent a good model for some aspects of LFS and LFL.

RS-SCID, another rare human disorder, is associated with hypomorphic mutations of ARTEMIS. Untreated RS-SCID patients usually succumb within 1 year of birth, but bone marrow transplantation has successfully restored immune function and extended survival in these patients (de Villartay *et al*., 2003). Furthermore, a recent preclinical study demonstrated that lentiviral-mediated gene transfer can also restore immune function in *Artemis* null (RS-SCID) mice and may represent an attractive alternative to conventional therapies (Mostoslavsky *et al*., 2006). Here, we have shown that deficiency for *Art* confers both lymphoid and non-lymphoid cancer risks in a *Trp53* compromised setting. Our data demonstrate that the possibility of non-lymphoid malignancies, especially in successfully immunorestored RS-SCID patients with increased longevity, is a potentially major clinical concern. It will be important to determine whether inherited polymorphisms affecting *TP53*, or p53-associated pathways, interact with Artemis deficiency to modulate disease susceptibility or specific pathology. In this context, $Art^{N/N}Trp53^{N/+}$ mice may also serve as a clinically relevant model to study the interplay of DSB repair and *TP53* in both lymphoid and non-lymphoid tumor suppression.

The p53 tumor suppressor determines event spectrum and sequence in multi-hit oncogenesis

Our data indicate that *Art*, and by extension NHEJ, is important for prevention of certain LOH events, and that spontaneously occurring DSBs can initiate loss of *Trp53* through allele replacement, at least in lymphocytes. Because complicon formation is an efficient transformation mechanism, we predicted that *Trp53* LOH, as an early transforming step, would lead to lymphomas identical to those in $Art^{N/N}Trp53^{N/N}$ mice (Zhu *et al*., 2002). However, this was not observed. Based on our observation that $Art^{N/N}Trp53^{LOH}$ pro-B cell lymphomas unexpectedly developed molecular and cytogenetic features distinct from those in $Art^{N/N}Trp53^{N/N}$ tumors, we now propose a refined model for multi-hit tumorigenesis. By this model, p53 status at the time of tumor initiation influences the order and timing of subsequent events, even if p53 function is

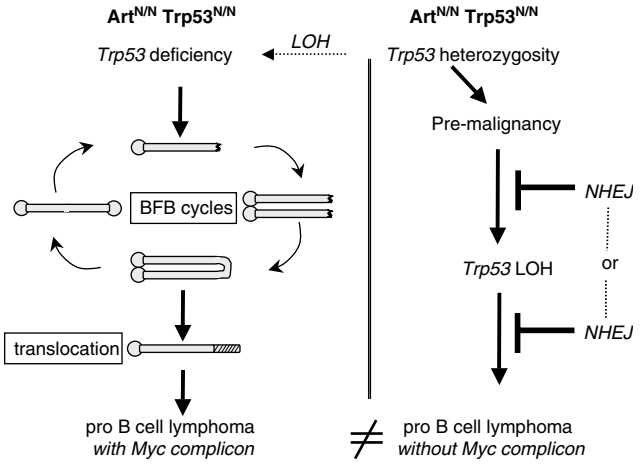

Figure 6 Model for lymphomagenesis associated with loss of *Trp53* heterozygosity. B-lineage cells that are deficient for both *Artemis* and *Trp53* undergo complicon formation via breakage-fusion-bridge (BFB) cycles, resulting in *Igh* and *c-myc* or *N-myc* co-amplification. By contrast, $Art^{N/N}Trp53^{N/+}$ cells B-lineage cells that acquire a premalignant state before *Trp53* LOH undergo subsequent oncogenic changes that are distinct from *Igh*/*Myc* complicon formation.

eventually lost (Figure 6). We propose that, before *Trp53* LOH, $Art^{N/N}Trp53^{N/+}$ cells acquire a premalignant state, perhaps by activation of a weak proto-oncogene (Figure 6). These cells become poised for full transformation but are prevented from overt neoplastic transformation through functional p53 activity. Abrogation of p53 by LOH then enables neoplastic progression and conversion to full malignancy. Complicon formation in $Art^{N/N}Trp53^{LOH}$ cells is circumvented because loss of p53 is sufficient for conversion to full malignancy, obviating the need for further oncogenic translocations or amplification. The rarity of complicon formation described in human tumors may, in part, be explained by the necessity for full loss of p53 function before the complicon-initiating translocation. In this regard, it is likely that the $Art^{N/N}Trp53^{LOH}$ tumorigenic mechanism described here more closely reflects many clinical situations, where partial p53 activity is retained, and is sufficient to resist complicon formation, thus favoring step-wise progression from premalignancy, through *TP53* LOH, to disease. In this context, it will be interesting to determine whether complicon rates differ in sporadic tumors from patients with intact *TP53* versus histologically similar tumors from LFS or LFL patients.

Clinical implications of this study

We show in this study that, in the absence of the NHEJ factor Artemis, multi-tissue tumorigenesis in a *Trp53* heterozygous context is accelerated and the tumor spectrum is shifted. It will be interesting to determine whether mutations in *Art* or other NHEJ genes similarly interact with p53 to confer tumor susceptibility in humans, and to evaluate their mechanistic roles in preventing formation of oncogenic chromosomal lesions such as complicons. In this context, $Art^{N/N}Trp53^{N/+}$ mice may represent a model for some RS-SCID patients, who are potentially at risk for development of several types of cancer, and may provide insight into the clinical heterogeneity observed in familial cancer syndromes such as Li-Fraumeni and Li-Fraumeni-like. Another important implication of this study is that p53 allelotype in RS-SCID or other NHEJ-related human immunodeficient patients could prove to be a key predictive factor in specific tumor susceptibility as these patients age (de Villartay *et al*., 2003).

Materials and methods

Mice heterozygous for a null allele of the gene encoding *Artemis* (*Dclre1c*/*Art*; Rooney *et al*., 2004b) were crossed with *Trp53* heterozygous mice to produce doubly heterozygous 129Sv/C57BL/6 $Art^{N/+}Trp53^{N/+}$ mice. These were backcrossed to C57BL/6 $Art^{N/N}$ mice, and progeny were crossed to generate $Art^{N/N}Trp53^{N/N}$ and $Art^{N/N}Trp53^{N/+}$ mice. Mice were regularly monitored and euthanized at the first sign of illness. Differences in survival for $Art^{N/N}Trp53^{N/+}$ and $Trp53^{N/+}$ cohorts were tested using a log-rank test of survival analysis in JMP6.0 (SAS Institute Inc., Cary, NC, USA).

Histology and flow cytometry

For histological analysis, tissues were fixed in Bouins fixative, paraffin embedded and sections stained with hematoxylin and eosin (H&E). Tumor tissue was processed for genomic DNA, total RNA and metaphase chromosome spreads (see below). Genomic DNA was prepared by phenol chloroform extraction and isopropanol precipitation. Tumor tissue was soaked overnight in RNALater, and stored at −20°C, or further processed by Trizol extraction, according to the manufacturer's protocol for total RNA isolation.

Single cell suspensions for flow cytometry were prepared by manual disruption of isolated tissue into RPMI media + 10% fetal calf serum. Cell suspensions were stained with either a B (IgM, B220, CD43, CD19) or T (CD3, CD4, CD8) cell diagnostic antibody cocktail. Flow cytometric analysis was performed using a Becton-Dickinson (Franklin Lakes, NJ, USA) FACSCalibur system operated with CellQuest Pro software, and analyzed using FlowJo2.0 software.

Spectral karyotyping and FISH

Metaphase chromosomes were prepared from freshly isolated lymphoma cells cultured for 3–6 h in the presence of 25 ng/ml IL-7 (R&D Systems, Minneapolis, MN, USA) and 50–100 ng/ml colcemid (KaryoMAX, GIBCO). Metaphase chromosome preparation and SKY analysis were performed as described previously (Sharpless *et al*., 2001). Fluorescence *in situ* hybridization was performed according to standard methods (Akeson *et al*., 2001, 2006). Slides were counterstained with DAPI and imaging was performed on a Nikon 90i upright fluorescence microscope or on an ASI cytogenetics workstation (Applied Spectral Imaging, Vista, CA, USA). The following probes were used for FISH. Chr 11: BAC1 = RP23-182G20, BAC2 = RP32402K16, BAC3 = RP23-211J23 and BAC4 = RP23-341I8; *c-myc*: RP23-130M17. The *Igh* specific BAC probe was described previously (Bassing *et al*., 2003).

Array CGH

Four micrograms of genomic DNA was labeled with either Cy3 or Cy5 by random octamer priming and extension,

according to manufacturer's protocols (Invitrogen; Carlsbad, CA, USA). Mouse Exon Evidence Based Oligonucleotide (MEEBO) Arrays (Microarrays Inc., Nashville, TN, USA) were simultaneously hybridized with 100 pmol each of labeled tumor and control DNA. Images were obtained using an Axon 4000B Scanner, and gridded and flagged by the spot finding feature of GenePix Software, version 5.1. For all tumors test-versus-reference hybridizations were performed in dye-swapped duplicates (Kerr and Churchill, 2001).

Quantitative PCR

CancerQuantArray, a high-throughput 384-well real-time PCR platform, was utilized to measure DNA copy number changes at selected cancer-related loci (Akilesh *et al*., 2003; Hart *et al*., 2004). Triplicate tumor DNA samples were compared with reference DNA. Cycle threshold (C_t) values were normalized using quantile normalizations, and copy number changes were estimated by ANOVA using R/Maanova (Irizarry *et al*., 2003; Wu *et al*., 2003; Churchill, 2004).

Trp53-specific quantitative PCR was performed using Power SYBR Green PCR Master Mix on ABI Real-Time PCR 7500 (Applied Biosystems, Foster City, CA, USA), with primers detecting a knockout allele specific sequence (NEO), a sequence shared by the wild type and null alleles (COMMON), or one of four reference sequences (Cd28, Lck, Prkcd, G22p1) (Supplementary Table 3; Supplementary methods).

Acknowledgements

We thank the members of the Mills lab, as well as Frederick Alt, Shaoguang Li, Mitch McVey and Lindsay Shopland for helpful comments and discussions, Kathy Snow for technical assistance, and Jin Szatkiewicz for statistical analysis. This work was supported by NIH grant R01 CA115665. SAM was supported by NIH Training Grant T32 HD07065-27. YHW was supported by NSF IGERT Training Grant 0221625 (University of Maine; Knowles, PI). D Roopenian and D Shaffer are founders of Bar Harbor Biotechnology.

References

Akeson EC, Donahue LR, Beamer WG, Shultz KL, Ackert-Bicknell C, Rosen CJ *et al*. (2006). Chromosomal inversion discovered in C3H/HeJ mice. *Genomics* **87**: 311–313.

Akeson EC, Lambert JP, Narayanswami S, Gardiner K, Bechtel LJ, Davisson MT. (2001). Ts65Dn – localization of the translocation breakpoint and trisomic gene content in a mouse model for Down syndrome. *Cytogenet Cell Genet* **93**: 270–276.

Akilesh S, Shaffer DJ, Roopenian D. (2003). Customized molecular phenotyping by quantitative gene expression and pattern recognition analysis. *Genome Res* **13**: 1719–1727.

Bassing CH, Suh H, Ferguson DO, Chua KF, Manis J, Eckersdorff M *et al*. (2003). Histone H2AX: a dosage-dependent suppressor of oncogenic translocations and tumors. *Cell* **114**: 359–370.

Churchill GA. (2004). Using ANOVA to analyze microarray data. *Biotechniques* **37**: 173–177.

de Villartay JP, Poinsignon C, de Chasseval R, Buck D, Le Guyader G, Villey I. (2003). Human and animal models of V(D)J recombination deficiency. *Curr Opin Immunol* **15**: 592–598.

Donehower LA, Harvey M, Slagle BL, McArthur MJ, Montgomery Jr CA, Butel JS *et al*. (1992). Mice deficient for p53 are developmentally normal but susceptible to spontaneous tumours. *Nature* **356**: 215–221.

Ege M, Ma Y, Manfras B, Kalwak K, Lu H, Lieber MR *et al*. (2005). Omenn syndrome due to ARTEMIS mutations. *Blood* **105**: 4179–4186.

Eilers PHC, de Menezes RX. (2005). Quantile smoothing of array CGH data. *Bioinformatics* **21**: 1146–1153.

Ferguson DO, Alt FW. (2001). DNA double strand break repair and chromosomal translocation: lessons from animal models. *Oncogene* **20**: 5572–5579.

Hart GT, Shaffer DJ, Akilesh S, Brown AC, Moran L, Roopenian DC *et al*. (2004). Quantitative gene expression profiling implicates genes for susceptibility and resistance to alveolar bone loss. *Infect Immun* **72**: 4471–4479.

Harvey M, McArthur MJ, Montgomery Jr CA, Butel JS, Bradley A, Donehower LA. (1993). Spontaneous and carcinogen-induced tumorigenesis in p53-deficient mice. *Nat Genet* **5**: 225–229.

Holcomb VB, Vogel H, Marple T, Kornegay RW, Hasty P. (2006). Ku80 and p53 suppress medulloblastoma that arise independent of Rag-1-induced DSBs. *Oncogene* **25**: 7159–7165.

Irizarry RA, Bolstad BM, Collin F, Cope LM, Hobbs B, Speed TP. (2003). Summaries of Affymetrix GeneChip probe level data. *Nucl Acids Res* **31**: e15.

Jacks T, Remington L, Williams BO, Schmitt EM, Halachmi S, Bronson RT *et al*. (1994). Tumor spectrum analysis in p53-mutant mice. *Curr Biol* **4**: 1–7.

Jackson SP. (2002). Sensing and repairing DNA double-strand breaks. *Carcinogenesi* **23**: 687–696.

Jasin M. (2000). Chromosome breaks and genomic instability. *Cancer Invest* **18**: 78–86.

Jeggo PA, Lobrich M. (2006). Contribution of DNA repair and cell cycle checkpoint arrest to the maintenance of genomic stability. *DNA Repair (Amst)* **5**: 1192–1198.

Jiang W, Ananthaswamy HN, Muller HK, Ouhtit A, Bolshakov S, Ullrich SE *et al*. (2001). UV irradiation augments lymphoid malignancies in mice with one functional copy of wild-type p53. *PNAS* **98**: 9790–9795.

Kerr MK, Churchill GA. (2001). Experimental design for gene expression microarrays. *Biostatistics* **2**: 183–201.

Lasko D, Cavenee W, Nordenskjold M. (1991). Loss of constitutional heterozygosity in human cancer. *Annu Rev Genet* **25**: 281–314.

Liang L, Shao C, Deng L, Mendonca MS, Stambrook PJ, Tischfield JA. (2002). Radiation-induced genetic instability *in vivo* depends on p53 status. *Mutation Research/Fundamental and Molecular Mechanisms of Mutagenesis* **502**: 69–80.

Mills KD, Ferguson DO, Alt FW. (2003). The role of DNA breaks in genomic instability and tumorigenesis. *Immunol Rev* **194**: 77–95.

Moshous D, Callebaut I, de Chasseval R, Corneo B, Cavazzana-Calvo M, Le Deist F *et al*. (2001). Artemis, a Novel DNA Double-Strand Break Repair/V(D)J Recombination Protein, Is Mutated in Human Severe Combined Immune Deficiency. *Cell* **105**: 177–186.

Moshous D, Pannetier C, Chasseval Rd R, Deist Fl F, Cavazzana-Calvo M, Romana S *et al*. (2003). Partial T and B lymphocyte immunodeficiency and predisposition to lymphoma in patients with hypomorphic mutations in Artemis. *J Clin Invest* **111**: 381–387.

Mostoslavsky G, Fabian AJ, Rooney S, Alt FW, Mulligan RC. (2006). Complete correction of murine Artemis immunodeficiency by lentiviral vector-mediated gene transfer. *Proc Natl Acad Sci U S A* **103**: 16406–16411.

Nicolas N, Moshous D, Cavazzana-Calvo M, Papadopoulo D, de Chasseval R, Le Deist F *et al*. (1998). A human severe combined immunodeficiency (SCID) condition with increased sensitivity to ionizing radiations and impaired V(D)J rearrangements defines a new DNA recombination/repair deficiency. *J Exp Med* **188**: 627–634.

Olivier M, Goldgar DE, Sodha N, Ohgaki H, Kleihues P, Hainaut P *et al*. (2003). Li-Fraumeni and related syndromes: correlation between tumor type, family structure, and TP53 genotype. *Cancer Res* **63**: 6643–6650.

Rooney S, Chaudhuri J, Alt FW. (2004a). The role of the nonhomologous end-joining pathway in lymphocyte development. *Immunol Rev* **200**: 115–131.

Rooney S, Sekiguchi J, Whitlow S, Eckersdorff M, Manis JP, Lee C *et al*. (2004b). Artemis and p53 cooperate to suppress oncogenic N-myc amplification in progenitor B cells. *Proc Natl Acad Sci U S A* **101**: 2410–2415.

Rooney S, Sekiguchi J, Zhu C, Cheng HL, Manis J, Whitlow S *et al*. (2002). Leaky Scid phenotype associated with defective V(D)J coding end processing in Artemis-deficient mice. *Mol Cell* **10**: 1379–1390.

Sharpless NE, Ferguson DO, O'Hagan RC, Castrillon DH, Lee C, Farazi PA *et al*. (2001). Impaired nonhomologous end-joining provokes soft tissue sarcomas harboring chromosomal translocations, amplifications, and deletions. *Mol Cell* **8**: 1187–1196.

Stark JM, Jasin M. (2003). Extensive loss of heterozygosity is suppressed during homologous repair of chromosomal breaks. *Mol Cell Biol* **23**: 733–743.

Tischfield JA, Shao C. (2003). Somatic recombination redux. *Nat Genet* **33**: 5–6.

Wu H, Kerr K, Cui X, Churchill GA. (2003). *The Analysis of Gene Expression Data: Methods and Software*. Springer: New York.

Yan CT, Kaushal D, Murphy M, Zhang Y, Datta A, Chen C *et al*. (2006). XRCC4 suppresses medulloblastomas with recurrent translocations in p53-deficient mice. *Proc Natl Acad Sci USA* **103**: 7378–7383.

Zhu C, Mills KD, Ferguson DO, Lee C, Manis J, Fleming J *et al*. (2002). Unrepaired DNA breaks in p53-deficient cells lead to oncogenic gene amplification subsequent to translocations. *Cell* **109**: 811–821.

Supplementary Information accompanies the paper on the Oncogene website (http://www.nature.com/onc).